1976 *Inorg. Chem.* **2010**, *49*, 1976–1982
DOI: 10.1021/ic902411h

Inorganic Chemistry
Article

A Family of Heteroleptic Titanium Guanidinates: Synthesis, Thermolysis, and Surface Reactivity

Yamile A. Wasslen,[†] Eva Tois,[‡] Suvi Haukka,[‡] Kevin A. Kreisel,[§] Glenn P. A. Yap,[§] Mathew D. Halls,[∥] and Seán T. Barry*,[†]

[†]*Department of Chemistry, Carleton University, 1125 Colonel By Drive, Ottawa, Ontario, Canada K1S 5B6,* [‡]*ASM Microchemistry, Väinö Auerin katu 12 A, Helsinki 00560, Finland,* [§]*Department of Chemistry and Biochemistry, University of Delaware, Newark, Delaware 19716, and* [∥]*Materials Science Division, Accelrys, Inc., San Diego, California 92121*

Received December 7, 2009

A family of new mixed-ligand titanium guanidinate compounds was synthesized as potential atomic layer deposition precursors, and the surface chemistry on silica of a promising candidate ($Cp_2Ti[(N^iPr)_2CN(H)^iPr]$) was explored. Generally, these compounds have very good thermal stability with onsets of volatility between 127 and 168 °C, with melting points generally ranging from 147 to 165 °C. The reactivity of $[^iPrN(H)C(N^iPr)_2]TiCp_2$ was studied with high surface area silica between 180 and 330 °C. The surface reactivity was found to differ if the silica was preheated to 350 or 900 °C; this was attributed to the hydroxyl nucleation site density of the silica, which is known to vary with the temperature. The surface reaction products were characterized by solid-state NMR, and these agreed well with a calculated model. When the silica was pretreated to 350 °C, the precursor appeared to chemisorb primarily through the loss of a Cp ligand, while with a 900 °C pretreatment, the chemisorption occurred primarily through a loss of the guanidinate ligand. The adsorption enthalpies to silica were calculated for the different surface species.

Introduction

Titanium-containing precursors find a variety of applications in microelectronics for the deposition of pure metal, nitride, and oxide. As a metal, titanium is used as a metal electrode, but due to its high tendency toward oxidation, titanium nitride is typically deposited as a capping layer.[1] The most important applications for titanium nitride are employment as an N-type gate metal and as a metal electrode in various capacitor applications, where it can be employed as pure TiN or mixed with aluminum or silicon.[2] In addition, thin films of TiN have been used in solar cells,[3] as hard and decorative coatings, and in optics.[4]

There is an increasing interest in titanium oxide due to its high *k* value. It can be deposited either as the pure oxide or with other oxides. For instance, with strontium oxide, it will form the ultra-high-*k* ternary material $SrTiO_3$, with a *k* value that may exceed 300. Titanium-based materials can be deposited by several known methods such as physical vapor deposition,[5] chemical vapor deposition (CVD),[6,7] and atomic layer deposition (ALD).[8] However, novel three-dimensional structures are an increasing trend in the semiconductor industry, and this calls for new ALD processes for the titanium based materials.

In ALD, $TiCl_4$ is the best-known titanium precursor. It is highly volatile and thermally stable. However, it cannot be used to deposit TiN layers at interconnects because of the formation of hydrogen chloride as a byproduct, which etches copper.[9] As well, $TiCl_4$ may induce the formation of a very stable $SrCl_2$ phase when employed in the deposition of $SrTiO_3$ by ALD.

Titanium alkyl amides have been studied in the deposition of TiN by ALD, but the drawback of this process is the low thermal stability of these precursors, which decompose above

*To whom correspondence should be addressed. E-mail: sbarry@ccs.carelton.ca.

(1) Grigorov, G. I.; Grigorov, K. G.; Stayanova, M.; Vignes, J. L.; Langeron, J. P.; Denjaean, P. *Appl. Phys. A: Mater. Sci. Process.* **1993**, *57*, 195.
(2) Shimizu, M.; Shiosaki, T. *Mater. Res. Soc. Symp. Proc.* **1995**, *361*, 295.
(3) Granqvist C. G. *Sol. Energy Mater. Sol. Cells* **2007**, *91*, 1529 and references therein.
(4) Perry, A. J.; Georgson, M.; Sproul, W. D. *Thin Solid Films* **1988**, *157*, 255.
(5) Wang, S.; Raaijmakers, I.; Burrows, B.; Suthar, S.; Redkar, S.; Kim, K. J. *Appl. Phys.* **1990**, *68*, 5176.
(6) Choy K. L. *Prog. Mater. Sci.* **2003**, *48*, 57 and references therein.
(7) Carmalt, C. J.; Newport, A. C.; O'Neill, S. A.; Parkin, I. P.; White, A. J. P.; Williams, D. J. *Inorg. Chem.* **2005**, *44*, 615.
(8) (a) Tiznado, H.; Menno Bouman, M.; Kang, B.-C.; Lee, I.; Zaera, F. *J. Mol. Catal. A: Chem.* **2008**, *281*, 35. (b) Kim, J.; Hong, H.; Oh, K.; Lee, C. *Appl. Surf. Sci.* **2003**, *210*, 231. (c) Ritala, M.; Leskelä, M.; Rauhala, E.; Haussalo, P. *J. Electrochem. Soc.* **1995**, *142*, 2731.
(9) Elers, K.-E.; Blomberg, T.; Peussa, M.; Aitchison, B.; Haukka, S.; Marcus, S. *Chem. Vap. Deposition* **2006**, *12*, 13.

Published on Web 01/12/2010

150 °C.[10,11] For TiO_2 deposition, there are a number of titanium precursors available: alkoxides have been used, but they are also not highly thermally stable. The highest temperatures they can withstand are around 250 °C.[12] A mixed imido, amido titanium precursor was shown to form tungsten carbide at low temperatures, but this required a plasma source.[13] Despite the large number of titanium precursors available for ALD, there is need for development of thermally stable metal organic titanium precursors for both TiN and TiO_2 deposition. In this paper, we introduce a new class of volatile and thermally stable titanium precursors for ALD: cyclopentadienyl titanium guanidinates.

An ALD precursor should meet several design criteria: the compound should have a low molecular weight, and the metal center should be sterically congested. This promotes volatility as well as self-limiting behavior when the chemisorbed monolayer is formed on the surface. The compound should be thermally stable to resist decomposition in the gas phase and on the surface at process temperatures, yet be chemically reactive to allow formation of the target film. Guanidinates are a class of ligands with rich connectivity and chemistry, and they have been used in several ALD and CVD precursors.[14] The flexibility of the guanidinate structure with respect to modifying its steric and electronic properties makes it a particularly useful ligand, and its well-known decomposition pathways allow chemical control of its thermal chemistry.

Herein, we report the synthesis and characterization of volatile heteroleptic titanium(III) precursor compounds $Cp_2Ti(N^iPr)_2CNRR'$ (where R, R'' = H, Me, ^{i}Pr). As well, we consider the volatility and thermal chemistry of these compounds to assess their suitability as ALD precursors. Finally, surface reactivity on high surface area silica is probed for the selected candidate $[^i PrN(H)C(N^iPr)_2]TiCp_2$ to determine how the precursor might dissociatively absorb to an oxide substrate. High surface area silica is an ideal material for this experiment due to the abundance of surface hydroxyls, which in turn lead to a high enough concentration of surface species to use solid-state nuclear magnetic resonance. The overall enthalpy of adsorption for the precursor on HO/SiO_2 is estimated from calculations employing a fully periodic surface model.

Results and Discussion

Generally, Ti(III) compounds of the formulation (guan)-$TiCp_2$ (where guan is any guanidinate) can be made in very low yield from Cp_2TiCl_2 and a dianionic guanidinate at room temperature with stirring overnight. There can be an in situ reduction of the titanium center, and the reaction mixture resulted in several unidentifiable side products. This reaction is highlighted here by using the compound $Cp_2Ti[(N^iPr)_2CN(H)^iPr]$ (**1**) as an example. When following the above route using $Li_2(^iPr(N)_3C)$ as a ligand, compound **1** was isolated in 15% yield, while the rational synthesis of **1** using Cp_2TiCl (from the reduction of Cp_2TiCl_2 with zinc dust) and $Li(^iPr(N)_2C(N(H)^iPr)$ produced **1** in 58% yield.

In general, compounds **1**−**4** were easily synthesized in moderate yields from the Cp_2TiCl starting material and appropriate lithium guanidinate. It was found that the compounds formed slowly at room temperature, with the starting titanium species changing from a characteristic yellow-green to a solution ranging from gray-green to blue, depending on the guanidinate. In every case, blue crystals were isolated, and this color change was used to gauge the completeness of the reaction. Compounds **1**−**3** produced crystals of sufficient quality for single-crystal structures to be collected (Figure 1 and Tables 1 and 2 for **1**, Figure 1 and Tables 1 and 3 for **2** and **3**).

In each structure, the titanium was in a four-coordinate, distorted tetrahedral environment considering the centroids of the cyclopentadienyl rings. Not surprisingly, the angle between the centroids was much larger than ideal (130−133°), and the bite angle of the guanidinate was correspondingly smaller (61.0−61.8°). The centroid−metal−nitrogen angles were closer to the ideal for **1** (108.4° and 109.8°) and **2** (109.5°) and somewhat distorted for **3** (111.4°). The guanidinate ring was very close to planar in each case, with torsion angles of 0−1.3°. As is typical for guanidinates, the exocyclic amido moieties were rotated from the plane of the guanidinate ring in all cases. However, π overlap follows a $\cos^2\theta$ relationship for twisted systems like this; thus the exocyclic group participated significantly in the delocalized π bonding of the guanidinate.[15] In every structure, the carbon−nitrogen bond to the exocyclic amide was longer than the carbon−nitrogen bonds to the chelate nitrogens. This bond indicated a higher contribution to the π system from the chelate ring compared to the exocyclic amide. This can be seen by the sum of angles around the chelate nitrogens on **1** an **2** (N1 at 360° and N2 at 359° for **1**, 360° for **2**), whose planarity indicated an sp^2 hybridization, and thus participation in the π system. Interestingly, compound **2** was defined by two planes of symmetry: one in the C1−Ti−C4 plane and one in the Ti−N1−C4 plane. This gives rise to two orientations of the isopropyl groups where they bend 14° above or below the Ti−N1−C4 plane 50% of the time. Likewise, the exocyclic amido group tilts 36° in either direction out of the C1−Ti−C4 plane 50% of the time. This symmetry is likely enforced by the crystal's $P4_2/ncm$ space group and forces the chelating nitrogen out of planarity.

In these structures, the bond lengths to the centroids were somewhat longer than a typical four-coordinate Cp titanium compound ($Cp_2Ti(NSO)_2$ reported by Roesky et al., Cp−Ti = 2.055)[16] and similar to those of the starting material $[Cp_2TiCl]_2$.[17] The Cp rings also showed a similar angle compared to the starting material (Cp−Ti−Cp = 131.2−133.4). The Ti−N bond lengths were within a typical bonding distance for a monoanionic guanidinate at titanium[18] and

(10) Leskalä, M.; Ritala, M. *Thin Solid Films* **2002**, *409*, 138.
(11) Elam, J. W.; Schuisky, M.; Ferguson, J. D.; George, S. M. *Thin Solid Films* **2003**, *436*, 145.
(12) (a) Pore, V.; Rahtu, A.; Leskela, M.; Ritala, M.; Sajavaara, D.; Keinonen, J. *Chem. Vap. Deposition* **2004**, *10*, 143. (b) Aktar, M. K.; Pratsinis, S. E.; Mastrangelo, S. V. R. *J. Mater. Res.* **1994**, *9*, 1241. (c) Evans, P.; Pemble, M. E.; Sheel, D. W. *Chem. Mater.* **2006**, *18*, 5750. (d) Kim, B. H.; Lee, J. Y.; Choa, Y. H.; Higuchi, M.; Mizutani, N. *Mater. Sci. Eng., B* **2004**, *107*, 289.
(13) Kim, D. H.; Kim, Y. J.; Song, Y. S.; Lee, B.-T.; Kim, J. H.; Suh, S.; Gordon, R. G. *J. Electrochem. Soc.* **2003**, *150*, C740.
(14) (a) Potts, S. E.; Carmalt, C. J.; Blackman, C. S.; Abou-chahine, F.; Pugh, D.; Davies, H. O. *Organometallics* **2009**, *28*, 1838. (b) Coyle, J. P.; Monillas, W. H.; Yap, G. P. A.; Barry, S. T. *Inorg. Chem.* **2008**, *47*, 683−689.
(15) DiLabio, G. A.; Litwinienko, G.; Shuquiong, L. S.; Pratt, D. A.; Ingold, K. U. *J. Phys. Chem. A* **2002**, *106*, 11719.
(16) Plenio, H.; Roesky, H. W.; Noltemeyer, M.; Sheldrick, G. M. J. *Chem. Soc., Chem. Commun.* **1987**, 1483.
(17) Jungst, R.; Sekutowski, D.; Davis, J.; Luly, M.; Stucky, G. *Inorg. Chem.* **1977**, *16*, 1645.
(18) Ong, T.-G.; Yap, G. P. A.; Richeson, D. S. *J. Am. Chem. Soc.* **2003**, *125*, 8100.

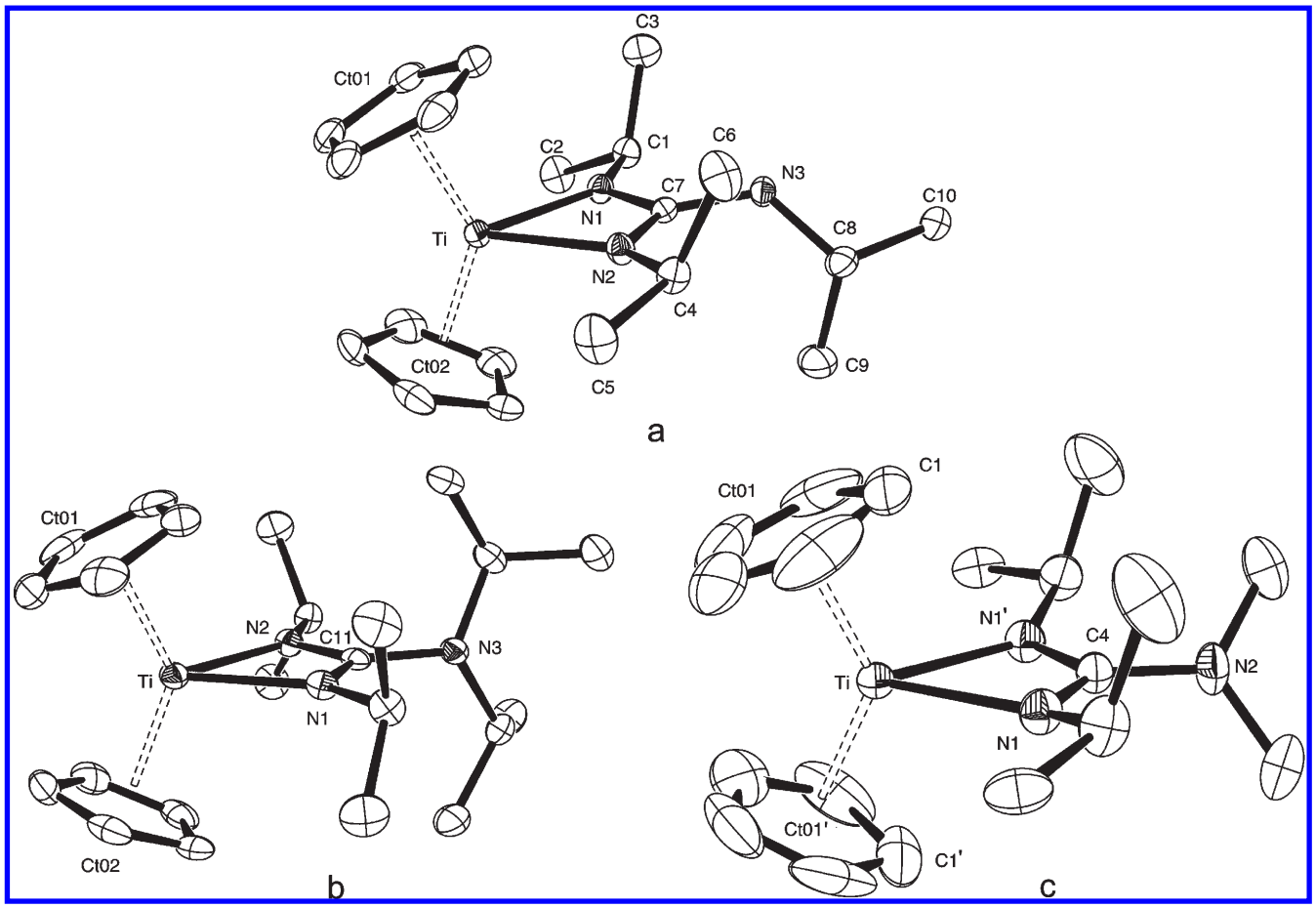

Figure 1. The single-crystal X-ray structures of (a) **1**, (b) **2**, and (c) **3**. The thermal ellipsoids are shown at 50% probability, and the hydrogen centers are omitted for clarity. N.B.: Only one of two orientations of **3** is shown (see text).

Table 1. Selected Crystal Data and Structure Refinement Parameters

empirical formula	$C_{20}H_{31}N_3Ti$ (**1**)	$C_{23}H_{38}N_3Ti$ (**2**)	$C_{19}H_{30}N_3Ti$ (**3**)
fw	361.38	404.46	348.36
T (K)	120	120	120
λ (Å)	0.71073	0.71073	0.71073
cryst syst	monoclinic	monoclinic	tetragonal
space group	$P2_1/n$	$P2_1/n$	$P4_2/ncm$
a (Å)	14.870	8.8431	8.1809
b (Å)	8.449	29.036	8.1809
c (Å)	16.922	9.0884	28.121
α (deg)	90	90	90
β (deg)	111.68	110.82	90
χ (deg)	90	90	90
V (Å^3)	1976	2181	1882
Z	4	4	4
ρ (calcd) (Mg/m^3)	1.215	1.232	1.229
abs coeff (mm^{-1})	0.439	0.405	0.458
refinement method	full-matrix least-squares on F2		
R indices [$I > 2\sigma(I)$][a]	R1 = 0.0505 wR2 = 0.1256	R1 = 0.0424 wR2 = 0.1064	R1 = 0.0578 wR2 = 0.1901

[a] $R1 = \sum||F_o| - |F_c||/\sum|F_o|$; $wR2 = (\sum w(|F_o| - |F_c|)^2/\sum w|F_o|^2)^{1/2}$.

also fell in the range reported by Hagadorn and Arnold for their prototypical titanium(III) amidinate (2.05−2.16 Å).[19]

The melting points of these compounds fell in a wide range, from 150 °C for **1** to decomposition at >180 °C for **2**. Thermogravimetric (TG) analysis showed all compounds to decompose with small, final residual masses and similar onsets of volatility (Figure 2, Table 4). The thermal data

Table 2. Experimental (XRD) Crystal Structure and BLYP/DNP Calculated Geometric Parameters for **1** as a Crystal and as a Gas-Phase Precursor[a]

	crystal (exptl)	crystal (calcd)	precursor (calcd)
	Bond Lengths (Å)		
C1−N1	1.463	1.46	1.47
C4−N2	1.464	1.47	1.47
C8−N3	1.479	1.49	1.49
C7−N1	1.339	1.35	1.35
C7−N2	1.341	1.35	1.35
C7−N3	1.405	1.40	1.41
N1−Ti	2.154	2.17	2.19
N2−Ti	2.147	2.17	2.21
Ct01−Ti	2.101	2.14	2.16
Ct02−Ti	2.091	2.13	2.16
N1−C7−N2	111.1	111.0	111.8
N1−C7−N3	122.4	122.8	121.7
N2−C7−N3	126.5	126.2	126.5
C7−N1−Ti	93.42	93.7	93.9
C7−N2−Ti	93.68	93.7	93.3
N2−Ti−N1	61.81	61.6	61.0
Ct01−Ti−Ct02	133.2	133.2	132.1
Ct01−Ti−N2	111.39	111.4	112.8
Ct01−Ti−N1	110.14	110.4	110.4
Ct02−Ti−N2	108.35	108.2	108.2
Ct02−Ti−N1	109.75	109.7	110.6
Ti−N1−C7−N2	1.3	0.8	0.4
N2−C7−N3−C8	45.6	42.9	44.0

[a] The atomic index corresponds to those shown in Figure 1a.

(19) Hagadorn, J. R.; Arnold, J. *Organometallics* **1998**, *17*, 1355.

Table 3. Selected Bond Lengths and Angles for Compounds **2** and **3**

$C_{23}H_{38}N_3Ti$ (**2**)		$C_{19}H_{30}N_3Ti$ (**3**)	
Selected Bond Lengths (Å)			
Ti−N1	2.1710(17)	Ti−N1	2.172(3)
Ti−N2	2.1730(17)		
N1−C11	1.326(3)	N1−C4	1.335(4)
N2−C11	1.328(3)		
N3−C11	1.433(3)	N2−C4	1.409(6)
Selected Bond Angles (deg)			
N1−Ti−N2	60.91(6)	N1−Ti−N1′	61.58(14)
Ct01−Ti−N1	109.5	Ct01−Ti-N1	111.4
Ct02−Ti−N2	109.5		
N1−C11−N2	112.14(17)	N1−C4−N1′	112.7(4)
N1−C11−N3	121.82(17)	N1−C4−N3	123.6(2)
N2−C11−N3	126.04(18)		
Sum of Angles (deg)			
N1	360	N1	356
N2	360	N2	360
N3	354		

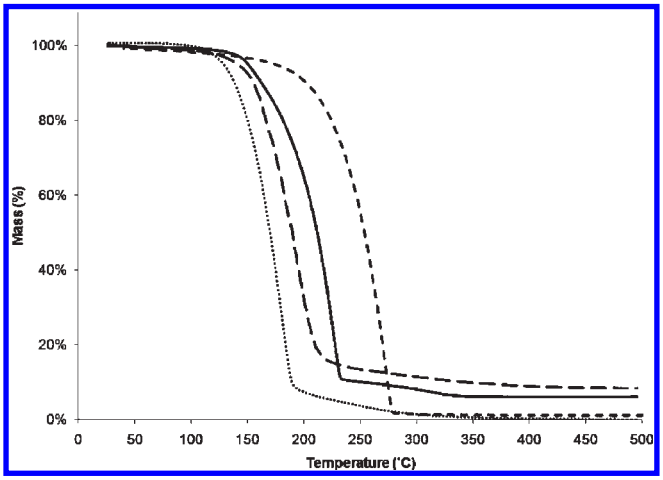

Figure 2. The thermogravimetric analysis of **1** (—), **2** (- - -), **3** (· · ·), and **4** (— —).

Table 4. Thermal Parameters for Compounds **1**−**4**

	exocyclic amido	melting point (°C)	onset of volatility[a] (°C)	residual mass (%)
1	R = ^{i}Pr, R′ = H	147−150	149	6.1
2	R = R′ = ^{i}Pr	decomposes > 180	168	1.3
3	R = R′ = Me	163−165	127	0.0
4	R = R′ = Et	155−157	139	8.5

[a] Onset of volatility was taken as a 5% mass loss.

showed no clear predominant candidate as an ALD precursor from these compounds, so compound **1** was selected due to its higher yield, lower melting point, and generally less problematic synthesis.

Closer thermal analysis was undertaken of compound **1**. There is a small initial weight loss in the TG of <1% (highlighted in the derivative curve) that is due to residual solvent in the sample. The onset of volatilization (i.e., 5% mass loss) occurred at 149 °C and showed an uninterrupted weight loss to 10.5% of the original mass. The differential curve for this weight loss had the typical appearance of sublimation, with an additional small feature centered at 155 °C: this interruption in the otherwise smooth volatilization

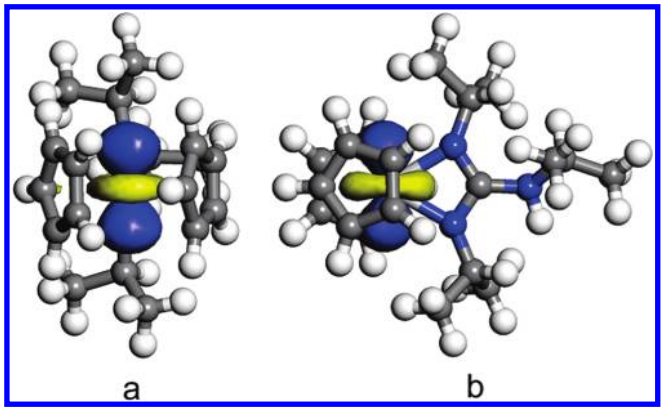

Figure 3. End-on (a) and side (b) views of the calculated highest occupied molecular orbital (HOMO) of **1** showing the localized d_{z^2} nature of the unpaired electron (0.04 e au^{-3}).

Table 5. Exposure Experiment Data for Silica Preheated at 350°C (SiO_2-350) and at 900°C (SiO_2-900)

substrate	reaction temperature (°C)	Ti density (at·nm-2)	C/Ti ratio
SiO_2-350	180	0.53	8.8
SiO_2-350	210	0.31	7.45
SiO_2-350	240	0.25	8.0
SiO_2-350	270	0.71	6.8
SiO_2-350	300	0.54	5.0
SiO_2-350	330	0.72	4.9
SiO_2-350	240	1.47	6.6
SiO_2-900	240	1.02	7.0

corresponds to the melting point of the sample and was likely caused by a change in surface area upon melting. From the residual mass after volatilization, there is a second weight loss of 4.4%. This could be the loss of volatility due to the presence of a nonvolatile impurity interrupting the kinetics of volatilization, or a subsequent thermal decomposition of the remaining material.

The differential scanning calorimetry (DSC) data for compound **1** suggested that the volatilization occurred while the material was in the liquid state. An initial endotherm at 152.5 °C corresponded to the melting point of **1**, as corroborated by benchtop methods. The second, broad endotherm corresponded to the major weight loss in the TG and can thus be assigned to the volatilization of the compound. Although the onset of volatilization was at a relatively high temperature with respect to ALD process temperatures, the lack of thermal decomposition during the volatilization event suggested that this material could be used as a vapor precursor.

Initial thermal ALD deposition experiments showed no appreciable film growth with **1** using water, oxygen, or air as a second precursor. Deposition temperatures up to 400 °C were attempted, and these experiments resulted in the condensation of compound **1** in the liquid nitrogen trap of the vacuum pump. This was surprising to us, since the compound shows appreciable reactivity to air when exposed under ambient conditions. Thus, we undertook an investigation of the surface reactivity of the precursor itself. We are continuing to investigate these precursors under a variety of harsher ALD conditions, including remote and direct plasma experiments.

Since compound **1** was pursued as a potential ALD precursor, solid-state and gas-phase optimized structures of

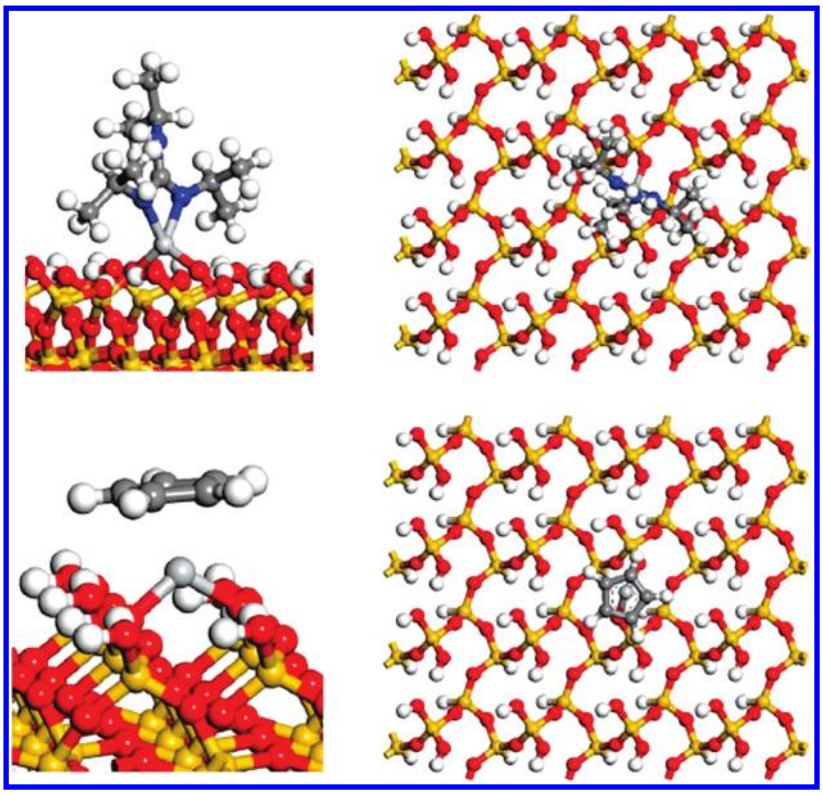

Figure 4. Side and top views (left and right panels, respectively) of the BLYP/DNP optimized surface reaction products for the [a] and [b] reaction pathways (top and bottom panels, respectively).

1 were calculated at the BLYP/DNP level of theory (selected parameters are included in Table 1). It was undertaken for use in surface reactivity studies (presented herein). The calculated and measured geometries are in good agreement, with an average difference for the periodic structural coordinates of 0.8 and 0.2%, for bond lengths and angles, respectively (Ti−Cp(crystal, calcd) = 2.14, 2.13 versus Ti−Cp-(X-ray) = 2.101, 2.091 Å; Ti−N(crystal, calcd) = 2.17, 2.17 versus Ti−N(X-ray) = 2.154, 2.147 Å). As expected, the agreement was slightly worse for the gas-phase calculated structure with average differences of 1.4 and 0.6%, for bond lengths and angles, respectively (Ti−Cp(gp, calcd) = 2.16, 2.16 versus Ti−Cp(X-ray) = 2.101, 2.091 Å; Ti−N(gp, calcd) = 2.19, 2.21 versus Ti−N(X-ray) = 2.154, 2.147 Å). The cyclopentadienyl groups, along with the monoanionic guanidinate chelating the metal center, gives rise to a doublet ground state for this system with the unpaired electron residing in the HOMO, which largely corresponds to the d_{z^2} orbital of the Ti(III) metal center, as depicted in Figure 3.

In potential ALD processes using **1** as a precursor, the initial nucleation pathway would involve nucleation on the interfacial oxide layer of a silicon substrate, creating a bound titanium complex. High surface area silica is the most often used material support for metallocene catalysts,[20] but it is a useful model to lend insight into the nucleation products at the interfacial oxide layer. High surface area silica is an ideal material for investigating the surface reactivity of **1** due to the abundance of surface hydroxyls, which in turn leads to a high enough concentration of surface species to use traditional characterization techniques such as (solid state) nuclear magnetic resonance.

Upon reactive exposure of the silica to a gas-phase metal precursor, the number of product surface species is directed by details of the surface structure. Preheating the substrate decreases the density of surface hydroxyl sites, limiting the coordination number of the bound product complex. Previous experimental work by Leskelä and co-workers,[21] using NMR and elemental analysis, demonstrated that the silica surface bonding mode of a zirconocene precursor depended on the level of substrate preheating.

We used silica pretreated at two different temperatures, 350 and 900 °C, called SiO_2-350 and SiO_2-900, respectively. In order to optimize the surface exposure experiment, SiO_2-350 was exposed to the titanium precursor in heated N_2 carrier gas for 5 h using 0.4−1.0 g of compound **1** at a variety of temperatures. In these cases, the precursor was completely volatilized from the bubbler. It was determined that 240 °C was the optimal temperature for the exposure experiments. When the reactions were repeated at 240 °C using an excess of precursor with substrates preheated at either 350 or 900 °C, complete saturation was visually evident from the change in color of the silica (Table 5).

SiO_2-350 turned uniformly bright orange, a color that persisted on air exposure. Solid-state NMR showed two ^{13}C resonances: a broad, complex peak in the aliphatic region centered at 23.8 ppm and a broad peak in the aromatic region at 115.3 ppm. Elemental analysis yielded a C/Ti ratio of 6.6. This suggests that **1** may decompose on the SiO_2-350 silica surface to yield both a guanidinate-containing as well as

(20) Fink, G.; Steinmetz, B.; Zechlin, J.; Przybyla, C.; Tesche, B. *Chem. Rev*. **2000**, *100*, 1377.

(21) Kröger-Laukkanen, M.; Peussa, M.; Leskelä, M.; Niinistö, L. *Appl. Surf. Sci*. **2001**, *183*, 290.

a Cp-containing surface species, suggesting that the surface enthalpies for eqs [a] and [b] are similar. SiO_2-900 was uniformly dark orange-brown, and this color faded to light yellow when the silica was exposed to the atmosphere for several hours. Solid-state ^{13}C NMR showed one resonance at 115.0 ppm, in the aromatic region, as well as a C/Ti ratio of 7.0. This suggested mainly a Cp−Ti surface complex.

To estimate the silica adsorption enthalpies of the doubly bonded surface species, calculations were carried at the BLYP/DNP level of theory for the following adsorption processes:

$$Cp_2TiGuan + 2SiO_2/OH \rightarrow SiO_2/(O)_2TiGuan + 2CpH \quad (a)$$

$$Cp_2TiGuan + 2SiO_2/OH \rightarrow SiO_2/(O)_2TiCp + CpH + GuanH \quad (b)$$

Typically, modeling a silicon surface means employing a Si_6 or Si_9 cluster, to minimize calculation time.[22] The calculation of reliable surface adsorption energies involving precursors containing bulky ligands requires the use of increasingly larger truncated surface models to ensure appropriate convergence of steric and electrostatic effects. The use of a fully periodic surface model ensures a physically realistic treatment of surface−adsorbate interactions. The model employed here consisted of a fully periodic 19.64 × 21.61 Å supercell of the hydroxylated (100)-α quartz surface having a stoichiometry of $Si_{48}O_{96}H_{64}$ (further details given in the Experimental Section). Such a model is expected to closely represent the vicinal OH reaction site on the 350 °C silica substrate, with a reactive OH distance of 3.5 Å. The gas-phase and surface reactant and product structures were fully optimized using an identical level of theory and convergence criteria. The final surface structures are shown in Figure 4. The top panels show the $SiO_2/(O)_2TiGuan$ complex, and the bottom panels show the $SiO_2/(O)_2TiCp$ complex. At the BLYP/DNP level of theory, both surface reaction pathways are found to be thermodynamically favorable. The overall computed reaction enthalpies for the surface reaction pathways [a] and [b] are remarkably similar, being −23.8 and −23.0 kcal/mol, respectively. The predicted enthalpies reported here are consistent with the experimental observation of both aliphatic and aromatic ligands retained on the surface titanium. A product ratio of 1:1 indicated by elemental analysis and NMR on the reaction products of **1** on the 350 °C preheated silica sample was found. We are presently investigating different surface models to better reflect the expected nonuniformity of a real high surface area silica substrate.

Conclusion

This work has presented the synthesis and structural characterization of a new monomeric Ti(III) gas-phase precursor, $Cp_2Ti[(N^iPr)_2CN(H)^iPr]$. The new precursor shows good volatility and thermal stability, satisfying important requirements for application as a titanium-containing precursor for chemical deposition techniques such as ALD. Silica exposure experiments at a relatively low substrate temperature, along with model DFT calculations, indicate that the precursor is reactive at surface nucleation sites, further supporting its utility for ALD or CVD applications.

Experimental Section

General Considerations. All manipulations were performed in a nitrogen-filled drybox. The chemicals, isopropyl amine, diisopropyl amine, diethyl amine, lithium dimethyl amide, methyl lithium, 1,3-diisopropyl carbodiimide, and zinc dust, were purchased from Aldrich Chemical Co. and used as received. Bis(cyclopentadienyl) titanium dichloride was purchased from StremChemicals and used without further purification. All solvents used were reagent-grade purified from an MBraun Solvent Purifier System. The monoanionic ligand synthesis of $[Me_2NC(N^iPr)_2]Li$, $[Et_2NC(N^iPr)_2]Li$, $[^iPr_2NC(N^iPr)_2]Li$, and $[^iPrN(H)C(N^iPr)_2]Li$ followed literature procedures.[23] Cp_2TiCl_2 was reduced to Cp_2TiCl following the literature procedure.[24] The dianonic ligand $Li_2(NiPr)_3C$ was prepared following the literature procedure.[25] Mass spectra were obtained using the electron impact method on a VG ZAB-2HF triple-focusing spectrometer. Guelph Chemical Laboratories performed combustion analysis. Thermogravimetric analysis was performed on a TA Instruments Q50 apparatus located within a Labmaster 130 Drybox. Differential scanning calorimetry was performed on a DSC Instruments Q10 apparatus.

Synthesis of $Cp_2Ti[(N^iPr)_2CN(H)^iPr]$ (1) from Cp_2TiCl_2. In a 60 mL round-bottom flask, 4.200 g (16.9 mmol) of bis-(cyclopentadienyl)titanium(IV) dichloride was allowed to stir in 40 mL of ether. A total of 3.326 g (16.9 mmol) of dianionic ligand was slowly added to the red solution. The solution changed from bright red to a dark maroon, almost brown color and was left to stir overnight. The solution was then filtered and placed in the freezer and allowed to sit for 24 h. A total of 0.916 g (2.53 mmol, 15% yield) of dark blue needle-like crystals of **1** was collected. Combustion analysis, found (calculated): C, 65.97 (66.29); H:, 9.21 (8.90); N, 11.52 (11.59). Mass spectral data (EI, *m*/*z*) (rel. intensity, %): 248 (100, M^+).

Synthesis of $Cp_2Ti[(N^iPr)_2CN(H)^iPr]$ (1) from Cp_2TiCl. A total of 2.82 g (9.88 mmol) of Cp_2TiCl was placed in a 60 mL round-bottom flask and dissolved in ether. To this solution, 1.89 g (9.88 mmol) of $LiN^iPrCN^iPr(N(H)^iPr)$ was slowly added. As the reaction proceeded, the solution changed from light green to dark blue. The reaction was allowed to stir overnight. It was then filtered to remove LiCl and placed in a freezer at −30 °C overnight. Thick dark blue needle-like crystals were collected at 58% yield (1.63 g, 5.73 mmol). Mass spectral data (EI, *m*/*z*) (rel. intensity, %): 248 (100, M^+). Combustion analysis, found (calculated): C, 65.87 (66.29); H, 9.23 (8.90); N, 11.65 (11.59).

Synthesis of $Cp_2Ti[(N^iPr)_2CN\ ^iPr_2]$ (2). In a 100 mL round-bottom flask, 3.79 g (17.8 mmol) of Cp_2TiCl was allowed to dissolve in about 60 mL of diethyl ether for about 10 min. An in situ solution of $[^iPr_2NC(N^iPr)_2]Li$ (4.14 g, 17.8 mmol) in diethyl ether was slowly added to the yellowish green titanium solution. The solution changed to a dark gray-green color. The reaction was allowed to stir overnight at room temperature. The green solution was then filtered to remove LiCl. The blue mother liqueur was evacuated to dryness and redissolved in diethyl ether and placed into a freezer at −30 °C. Blue crystals were collected (3.74 g, 9.25 mmol), yielding 52%. Mass spectral data (EI, *m*/*z*; rel. intensity, %): 404.3 (100, M^+). Combustion analysis, found (calculated): C, 68.40 (68.30); H, 9.56 (9.47); N, 10.35 (10.39).

(22) For example, see: Haran, M.; Engstrom, J. R.; Clancy, P. *J. Am. Chem. Soc.* **2006**, *128*, 836.

(23) Aeilts, S. L.; Coles, M. P.; Swenson, D. C.; Jordan, R. F. *Organometallics* **1998**, *17*(15), 3265.

(24) Green, M. L. H.; Lucas, C. R. *J. Chem. Soc., Dalton Trans.* **1972**, 1000.

(25) Tin, M. K. T.; Yap, G. P. A.; Richeson, D. S. *Inorg. Chem.* **1998**, *26*, 6728.

Synthesis of $Cp_2Ti[(N^iPr)_2CNMe_2]$ (3). In a 60 mL round-bottom flask, 1.00 g (3.5 mmol) of Cp_2TiCl was allowed to dissolve in about 30 mL of diethyl ether for about 10 min. An in situ solution of $[Me_2NC(N^iPr)_2]Li$ (0.62 g, 3.5 mmol) in diethyl ether was slowly added to the yellowish green titanium solution. The reaction was allowed to stir overnight at room temperature. The baby blue solution was then filtered and evacuated to dryness and redissolved in approximately 5 mL of diethyl ether and placed into a freezer at −30 °C. A total of 0.52 g (1.49 mmol) of a baby blue solid was collected, resulting in 43% yield. Mass spectral data (EI, *m*/*z*; rel. intensity, %): 348 (37.3, M^+). Combustion analysis, found (calculated): C, 65.85 (65.51); H, 9.00 (8.68); N, 11.64 (12.06).

Synthesis of $Cp_2Ti[(N^iPr)_2CNEt_2]$ (4). In a 60 mL round-bottom flask, 1.00 g (3.5 mmol) of Cp_2TiCl was allowed to dissolve in about 30 mL of diethyl ether for about 10 min. An in situ solution of $[Et_2NC(N^iPr)_2]Li$ (0.719 g, 3.5 mmol) in diethyl ether was slowly added to the yellowish green titanium solution. The reaction was allowed to stir overnight at room temperature. The light blue solution was then filtered to remove LiCl, evacuated to dryness, and redissolved in approximately 5 mL of diethyl ether and placed into a freezer at −30 °C. A total of 0.57 g (1.5 mmol) of a dark blue solid was collected, resulting in 43% yield. Mass spectral data (EI, *m*/*z*; rel. intensity, %): 376 (100, M^+). Elem anal. exptl (calcd): C, 67.20 (67.01); H, 9.33 (9.11); N, 11.00 (11.16).

Exposure Experiments. The Ti guanidinate reactions were carried out using a commercial F120 ALCVD reactor manufactured by ASM Microchemistry Ltd. and equipped with a reaction chamber for processing porous materials. In the test exposures, 3 to 5 g of porous high surface area SiO_2 powder (Table 6) were heat-treated in a muffle furnace for 16 h at 350 or 900 °C. These were subsequently used as substrates. Before the introduction of the titanium precursor to the surface, the substrates were further preheated in the reaction chamber at the reaction temperatures for 3 to 5 h to remove any possible moisture adsorbed to the surface during storage. After the pretreatment, the Ti precursor was vaporized and transported with the help of nitrogen flow through the silica particles where it reacted. In the tests, just one exposure of the precursor was carried out on the oxide surface. The precursor amount was varied from 0.4 to 2.5 g, and the reaction time was 4 h to ensure surface saturation. The reaction temperatures studied were 180, 210, 240, 270, 300, and 330 °C. After the reaction, the reaction chamber was purged with nitrogen. The samples were handled inertly by storing them in the glovebox.

The samples were characterized by elemental analysis and solid-state NMR spectroscopy. Titanium content was determined by instrumental neutron activation analysis, and carbon content was determined with a Leco CR12 carbon analyzer. Solid-state ^{13}C NMR was performed on a Bruker AVANCE 500 NMR spectrometer.

(26) Sheldrick, G.M. *Acta Crystallogr., Sect. A* **2008**, *64*, 112.

Table 6. Physical Properties of High Surface Area SiO_2 Substrate

oxide	type	surface area (m^2/g)	pore volume (cm^3/g)	pore size (nm)	mean particle diameter (μm)
SiO_2	INEOS silicas EP10X	300	1.8	24	100

Structural Determination. A suitable single crystal was selected and mounted on a glass fiber using Paratone oil, flash-cooled to 150 K. Data were collected on a Brüker-AXS APEX CCD diffractometer with graphite-monochromated Mo Kα radiation (λ = 0.71073 Å). Unit cell parameters were obtained from 60 data frames, 0.3° ω, from three different sections of the Ewald sphere. The systematic absences in the data and the unit cell parameters were uniquely consistent with the reported space group. The data set was treated with SADABS absorption corrections based on redundant multiscan data.[26] All non-hydrogen atoms were refined with anisotropic displacement parameters. All hydrogen atoms were treated as idealized contributions. Structure factors are contained in the SHELXTL 6.12 program library.[26]

Computational Methods. Calculations were carried out using the gradient-corrected B-LYP density functional, corresponding to Becke's exchange functional[27] (B) in combination with the Lee−Yang−Parr correlation functional[28] (LYP), as implemented in the *DMol3* package.[29] A spin unrestricted electronic scheme using a numerical atomic basis set of double-ζ quality, augmented with additional polarization functions (DNP) with a real-space cutoff of 6.0 Å, was employed in this work. For Ti, the core electrons were represented with an effective relativistic semicore pseudopotential[30] along with the DNP basis for valence electrons. The convergence criteria for structural optimizations were 1.0×10^{-5} au and 2.0×10^{-3} au/Å for the energy and gradient, respectively. Surface calculations were based on a hydrogen-terminated, four-layer slab of the (100)-α quartz surface using a 4 × 4 supercell (19.64 Å × 21.61 Å) with a 30 Å vacuum slab. For the bulk and surface periodic calculations, a Monkhorst-Pack *k*-point mesh with a spacing of 0.04 $Å^{-1}$ was used to sample the Brillouin zone.

Acknowledgment. We thank the Natural Sciences and Engineering Research Council of Canada (NSERC Discovery Grants, S.T.B.). We thank Dr. Glenn Facey at the University of Ottawa for assistance with the solid-state NMR.

Supporting Information Available: Crystallographic data for compounds **1**−**3**. This information is available free of charge via the Internet at http://pubs.acs.org.

(27) Becke, A. D. J. *Chem. Phys.* **1988**, *88*, 2547.
(28) Lee, C.; Yang, W.; Parr, R. G. *Phys. Rev. B* **1988**, *37*, 786.
(29) Delley, B. *J. Chem. Phys.* **2000**, *113*, 7756.
(30) Delley, B. *Phys. Rev. B* **2002**, *66*, 155125.